Original Article

MOLECULAR METABOLISM

Ablation of ORMDL3 impairs adipose tissue thermogenesis and insulin sensitivity by increasing ceramide generation

Yu Song [1,5], Wenying Zan [1,5], Liping Qin [1], Shuang Han [1], Lili Ye [2], Molin Wang [1], Baichun Jiang [1], Pan Fang [3], Qiji Liu [1], Changshun Shao [4], Yaoqin Gong [1,], Peishan Li [1,4,*]**

ABSTRACT

Objective: Genome-wide association studies identified *ORMDL3* as an obesity-related gene, and its expression was negatively correlated with body mass index. However, the precise biological roles of ORMDL3 in obesity and lipid metabolism remain uncharacterized. Here, we investigate the function of ORMDL3 in adipose tissue thermogenesis and high fat diet (HFD)-induced insulin resistance.

Methods: *Ormdl3*-deficient (*Ormdl3*$^{-/-}$) mice were employed to delineate the function of ORMDL3 in brown adipose tissue (BAT) thermogenesis and white adipose tissue (WAT) browning. Glucose and lipid homeostasis in *Ormdl3*$^{-/-}$ mice fed a HFD were assessed. The lipid composition in adipose tissue was evaluated by mass spectrometry. Primary adipocytes in culture were used to determine the mechanism by which ORMDL3 regulates white adipose browning.

Results: BAT thermogenesis and WAT browning were significantly impaired in *Ormdl3*$^{-/-}$ mice upon cold exposure or administration with the β3 adrenergic agonist. In addition, compared to WT mice, *Ormdl3*$^{-/-}$ mice displayed increased weight gain and insulin resistance in response to HFD. The induction of uncoupling protein 1 (UCP1), a marker of thermogenesis, was attenuated in primary adipocytes derived from *Ormdl3*$^{-/-}$ mice. Importantly, ceramide levels were elevated in the adipose tissue of *Ormdl3*$^{-/-}$ mice. In addition, the reduction in thermogenesis and increase in body weight caused by *Ormdl3* deficiency could be rescued by inhibiting the production of ceramides.

Conclusion: Our findings suggest that ORMDL3 contributes to the regulation of BAT thermogenesis, WAT browning, and insulin resistance.

Keywords ORMDL3; Thermogenesis; Beige fat; Insulin resistance; Ceramide; Brown adipose tissue

1. INTRODUCTION

Obesity, which occurs as a consequence of a disturbed energy balance due to increased energy intake and/or lowered energy expenditure, dramatically increases the risk of developing many life-threatening diseases such as diabetes, heart disease, and stroke [1]. Adipose tissues play an important role in regulating systemic energy homeostasis. Adipocytes can be divided into three types: white, brown, and beige adipocytes, according to the number/size of lipid droplets, mitochondrial density and thermogenic capacity. While white adipocytes store excess energy as large, unilocular lipid droplets, brown and beige adipocytes dissipate energy by producing heat through adaptive nonshivering thermogenesis [2]. The mitochondria in brown/beige adipocytes are enriched in uncoupling protein 1 (UCP1), which is localized on the inner membrane of mitochondria. When activated, UCP1 uncouples oxidation and phosphorylation of the respiratory chain and consumes energy by generating heat [3]. Recent studies indicate that brown/beige adipocytes are crucial in the regulation of energy expenditure and that stimulating brown/beige adipocyte formation and activity represents a potential and promising therapeutic strategy to combat obesity and the associated metabolic diseases, including type 2 diabetes [4,5]. However, well-defined pathways or targets suitable for pharmacological intervention are lacking at present.

ORMDL3 is one member of the orosomucoid-like (*ORMDL*) gene family (*ORMDL1-3*) and encodes endoplasmic reticulum (ER)-localized proteins. Recent studies indicate that *ORMDL3* gene polymorphisms are associated with a diverse set of inflammatory diseases, including bronchial asthma [6], type 1 diabetes [7], inflammatory bowel diseases

[1]The Key Laboratory of Experimental Teratology, Ministry of Education and Department of Molecular Medicine and Genetics, School of Basic Medical Sciences, Cheeloo College of Medicine, Shandong University, Jinan, Shandong, 250012, China [2]Department of Special Examination, The Affiliated Hospital of Shandong University of Traditional Chinese Medicine, Jinan, Shandong, 250011, China [3]Department of Biochemistry and Molecular Biology, Soochow University Medical College, Suzhou, Jiangsu, 215123, China [4]State Key Laboratory of Radiation Medicine and Protection, Institutes for Translational Medicine, Soochow University Medical College, Suzhou, Jiangsu, 215123, China

[5] Yu Song and Wenying Zan contributed equally.

*Corresponding author. Institutes for Translational Medicine, Soochow University Medical College, Suzhou, Jiangsu, 215123, China. E-mail: psli@suda.edu.cn (P. Li).

**Corresponding author. Department of Molecular Medicine and Genetics, School of Basic Medical Sciences, Cheeloo College of Medicine, Shandong University, Jinan, Shandong, 250012, China. E-mail: yxg8@sdu.edu.cn (Y. Gong).

Received July 1, 2021 • Revision received December 16, 2021 • Accepted December 17, 2021 • Available online 22 December 2021

https://doi.org/10.1016/j.molmet.2021.101423

[8], ankylosing spondylitis [9], and atherosclerosis [10]. The possible mechanisms of ORMDL3 in regulating inflammation include altering ER-mediated calcium (Ca^{2+}) homeostasis [11], facilitating the unfolded protein response [12], and inducing cellular stress responses [13]. Importantly, recent genome-wide association studies identified *ORMDL3* as an obesity-related gene, and its expression was negatively correlated with body mass index [14]. However, the precise biological roles of ORMDL3 in obesity and lipid homeostasis remain to be characterized.

In this study, we found that BAT thermogenesis and WAT browning were attenuated in *Ormdl3*$^{-/-}$ mice. Depletion of *Ormdl3* impaired the differentiation of preadipocytes into thermogenically competent beige/brown-like adipocytes *in vitro*. *Ormdl3*$^{-/-}$ mice were sensitive to HFD-induced obesity and insulin resistance. Mechanistically, we demonstrated that *Ormdl3* deficiency impaired adipose tissue thermogenesis and insulin sensitivity by increasing ceramide generation.

2. MATERIALS AND METHODS

2.1. Animals

All animal experiments were performed in accordance with protocols approved by the Institutional Animal Care and Use Committee, Shandong University, School of Basic Medical Sciences. *Ormdl3* whole body knockout (*Ormdl3*$^{-/-}$) mice on a C57BL/6 background have been previously described [15]. Unless otherwise specified, the mice were housed in a specific-pathogen-free facility in plastic cages at 22 °C and 40—50% humidity, with a daylight cycle from 6:00 AM to 6:00 PM. All mice used in these studies were male maintained on standard chow diets or fed a 60 kcal% high fat diet (HFD; Research Diets, D12492) ad libitum. For studies at thermoneutrality or involving cold exposure, 8-week-old mice were housed in an environmental chamber set to either 30 °C (thermoneutrality) or 4 °C (cold exposure) for 2 weeks. Rectal temperatures were measured using a dual channel Traceable Expanded Range Probe (Fisher Scientific), and food was provided during the measurement. CL316243 (MCE, HY-116771A) was injected intraperitoneally at the dose of 1 mg/kg/day for 5 days. The mice were sacrificed for analysis on the 6th day. Myriocin was injected intraperitoneally at the dose of 0.3 mg/kg every 2 days.

2.2. Metabolic studies

Mice were fasted overnight (12 h), and tail vein blood was collected. Plasma samples were stored at −20 °C until use. Concentrations of insulin (Abcam, ab277390), leptin (Abcam, ab100718), and adiponectin (Abcam, ab108785) were measured using ELISA kits. Concentrations of total cholesterol, triglyceride, and free fatty acid were measured using assay kits (Wako Diagnostics). For glucose tolerance test, mice were fasted overnight and then treated with an intraperitoneal injection of 0.75 g/kg glucose, followed by measurement of blood glucose levels with a glucometer (Roche). To assess insulin tolerance, mice were fasted for 4 h before receiving an intraperitoneal injection of insulin (1.5 units/kg body weight) and were then subjected to measurement of blood glucose levels.

2.3. Isolation of stromal-vascular fraction (SVF) from adipose tissues

Primary adipogenic precursor cells were isolated from ingWAT of 8-week-old mice. Adipose tissues were dissected from mice, rinsed in PBS, minced, and digested for 40 min at 37 °C in 0.1% (w/v) type I collagenase solution (Thermo Fisher Scientific, 17018029) with Hank's Balanced Salt Solution. Digested tissue was filtered through a 100-μm cell filter and centrifuged at 1200 rpm for 5 min. The sediment was resuspended and cultured in Dulbecco's modified Eagle's medium (DMEM, Gibco) with 10% fetal bovine serum.

For adipocyte differentiation assays, cells were grown to confluence and then treated with differentiation induction medium (DMEM/F12 with 10% FBS, 2 μg/ml dexamethasone, 0.5 mM isobutylmethylxanthine, 125 μM indomethacin, 20 nM insulin, and 1 nM T3; the above chemicals were purchased from Sigma). Induction medium was removed after 48 h, and cells were then grown in DMEM/F12 medium containing 10% FBS, 1 nM T3, and 5 μg/ml insulin until they were harvested. To stimulate a thermogenic program, cells were incubated either with 10 mM isoproterenol for 3 h or with 1 mM rosiglitazone for the entire differentiation time course. For Oil Red O staining, cell cultures were washed with PBS, fixed with 4% paraformaldehyde for 15 min, and stained with Oil Red O solution (Sigma, MAK194) for 30 min. All primary cell experiments were performed in 3 or 4 technical replicates.

2.4. H&E staining and immunohistochemistry

The adipose tissues were collected in 4% paraformaldehyde and incubated for 48 h at room temperature with gentle shaking. Paraffin-embedded adipose tissues were cut into 5-μm-thick sections, adhered onto glass slides, deparaffinized, and rehydrated by decreasing ethanol concentrations. Tissue-embedded slides were stained with hematoxylin and eosin (H&E). For immunohistochemistry, rehydrated tissues were washed with PBS, boiled in a citrate solution, and blocked with 4% serum before overnight incubation at 4 °C with primary antibodies against UCP1 (Cell Signaling, 72298) followed by horseradish peroxidase labeled secondary antibodies (SP-9000, ZSGB-Bio). The slides were thoroughly washed and counterstained with hematoxylin, and then examined under a microscope (Olympus).

2.5. Western blot analysis

The adipose tissues were lysed in RIPA buffer containing 0.5% NP-40, 0.1% sodium deoxycholate, 150 mM NaCl, 50 mM Tris-Cl, pH 7.5, protease inhibitor cocktail (Complete, Roche), and 1 mM phenylmethylsulfonyl fluoride. Protein concentrations were quantified using a detergent-compatible protein assay kit (Bio-Rad). Lysates were run on Bis-Tris gels, transferred to a PVDF membrane (Millipore), and probed with primary antibodies. The following antibodies were used: rabbit anti-UCP1 (Cell Signaling, 72298), mouse anti-Actin (Millipore, MAB1501), and mouse anti-PGC1α (Sigma, ABE868). Goat-anti-rabbit IgG conjugated to horseradish peroxidase (Cell Signaling Technology) was used as the secondary antibody.

2.6. Quantitative PCR assay

Total RNA was extracted with TRIzol reagents (Invitrogen). For mRNA analysis, 1 μg of total RNA was reverse transcribed by using a Revert Aid first strand cDNA synthesis kit (Roche). The cDNA was analyzed using Power SYBR green PCR master mix (Roche) with a Roche 480 system. The mRNA quantitative PCR data were normalized to *Gapdh*. Primer sequences are listed in Supplementary Table 1.

2.7. LC-MS/MS technology for non-targeted lipidomics analysis

The freshly isolated WAT was immediately frozen in liquid nitrogen and stored at −80 °C until use. Non-targeted lipidomics was performed by Beijing Genomics Institute. Briefly, 25 mg of samples were added to 800 μL of precooled methylene chloride/methanol (3:1, V: V) and 10 μL of SPLASH internal standard (330707, SPLASH™ Lipidomix Mass Spec Standard, Avanti Polar Lipids, including LPC 18:1(d7), LPE 18:1(d7), PC 15:0—18:1(d7), PE 15:0—18:1(d7), PG 15:0—18:1(d7), PS 15:0—18:1(d7), PI 15:0—18:1(d7), PA 15:0—18:1(d7), SM d18:1—18:1(d9),

cholesterol(d7), CE 18:1(d7), MG 18:1(d7), DG 15:0—18:1(d7) and TG 15:0—18:1(d7)—15:0 storage solution. The SPLASH internal standard was used for the evaluation of instrument stability. After grinding (50 Hz, 5 min) and ultrasonic treatment in a water bath for 10 min (4 °C), the samples were centrifuged at 25,000 rpm for 15 min. The supernatant was collected and dried using a vacuum centrigator. Next, 200 μL of isopropanol: acetonitrile: H_2O (2:1:1, V: V: V) was added, and the sample was vortexed for 1 min followed by sonication for 10 min. After centrifugation at 25,000 rpm for 15 min, the supernatant was collected and placed in sample tubes for LC-MS analysis. Next, 20 μL of supernatant from each sample was pooled as a quality control sample (QC) to evaluate LC-MS reproducibility and stability.

The Waters 2D UPLC (Waters, USA) and Q Exactive high resolution mass spectrometer (Thermo Fisher Scientific, USA) were used in this study for the measurement of metabolites. In positive mode, buffer A consisted of 10 mM ammonium formate, 0.1% formic acid, 60% acetonitrile and buffer B consisted of 10 mM ammonium formate, 0.1% formic acid, 90% isopropanol, and 10% acetonitrile. In negative mode, buffer A consisted of 10 mM ammonium formate, 60% acetonitrile and buffer B consisted of 10 mM ammonium formate 90% isopropanol, 10% acetonitrile. The gradient was as follows: 0—2 min, 40—43% buffer B, 2—2.1 min 43%—50% buffer B, 2.1—7 min 50%—54% buffer B, 7—7.1 min 54%—70% buffer B, 7.1—13 min 70%—99% buffer B, 13—13.1 min 99%—40% buffer B, 13.1—15 min 40% buffer B. The flowrate was 0.35 ml/min, and column temperature was set at 55 °C. The injection volume was 5 μL.

MS parameters: In MS1, mass range was 200—2000 *m/z*, resolution was 70 k, AGC was 3e6 and injection time was 100 ms. The top three intense precursors were selected for MS2. In MS2 method, the resolution was 17.5 K; AGC was 1e5; the injection time was 50 ms; and the stepped collision energy was 15, 30, and 45 eV. The ESI parameters were as follows: sheath gas flow rate was 40, aux gas flow rate was 10, and spray voltage was 3.8 in the positive mode and 3.2 in the negative mode. The capillary temperature was 320 °C, and the aux gas heater temperature was 350 °C.

Lipid Search 4.1 software was used for LC-MS/MS data processing, including a series of analyses such as intelligent peak extraction, lipid identification, and peak alignment. The parameters for lipid search include that the identification type is "product". The mass tolerance for precursor and product ions was 5 ppm. The peak area for all identified lipids were extracted using 5 ppm mass tolerance. The filter was set as "top rank", "all isomer peak" and "FA priority". M score was 5.0 and c-score was 2.0. The identification levels were classified into A, B, C, and D. The in-house metabolomics R software package metaX [16] was used for statistical analysis. Lipids with more than 50% missing values in the quality control samples and more than 80% missing values in the samples were deleted. The K-nearest neighbor algorithm was used for missing value imputation [17]. The QC samples were used for the probabilistic quotient normalization (PQN) [18]. Principal Component Analysis was used to observe the differences between the groups of the samples, and the Variable Importance in the Projectior (VIP) values of the first two principal components of the PLS-DA [19,20] model were used to screen different lipid molecules combined with multiple analyses of the difference change and the t test.

2.8. Data analysis

All data are presented as mean ± SEM or mean ± SD. Data were analyzed using Excel or GraphPad Prism 7.0. Values were compared using an unpaired nonparametric test (Mann—Whitney) to compare two groups or ordinary one-way ANOVA with Tukey's multiple comparisons test to compare the variance in three or more groups with one independent factor (e.g., treatment group). When there were effects of two factors (e.g., treatment and time) on a dependent variable, two-way ANOVA with Šidák's multiple comparisons test was employed. A p value < 0.05 was considered significant, whereas $p > 0.05$ was considered to be nonsignificant.

3. RESULTS

3.1. The expression of *Ormdl3* is downregulated in obese mice and humans and upregulated in response to cold exposure

To investigate the physiological function of ORMDL3, we first examined the expression of ORMDL3 in different mouse tissues. Currently, there are no commercially available antibodies that can detect specific expression of individual ORMDL family members. Therefore, we designed 3 pairs of primers that amplify each of the *Ormdl* genes specifically and confirmed their specific amplifications by sequencing the PCR products. The highest expression of *Ormdl3* was found in interscapular BAT (iBAT), while specific WAT depots (inguinal, ingWAT; epididymal, eWAT) showed lower but still relevant expression (Figure 1A), suggesting that ORMDL3 may play a unique role in the main functions of BAT, such as thermogenesis. Interestingly, the transcription levels of *Ormdl3* were significantly downregulated in the WAT and iBAT of HFD-induced obese mice and leptin receptor mutant (*db/db*) mice, compared with those from NCD-fed mice or WT mice, respectively (Figure 1B,C). To determine the clinical relevance of ORMDL3 expression, subcutaneous fat depots from humans with different body mass index (BMI) were obtained during surgery and analyzed. The mRNA levels of *ORMDL3* were significantly decreased in obese subjects and negatively correlated with BMI (Figure 1D), which was consistent with the previous report [14]. In addition, cold exposure markedly upregulated the expression of *Ormdl3*, but not *Ormdl1* or *Ormdl2*, in the WAT and iBAT of mice (Figure 1E). Taken together, these data suggest that ORMDL3 may be involved in the adaptive thermogenesis of fat tissues.

3.2. Depletion of *Ormdl3* impairs the thermogenic function of BAT

To investigate the physiological function of ORMDL3, previously reported *Ormdl3*-deficient ($Ormdl3^{-/-}$) mice were employed [15]. The *Ormdl3* expression in $Ormdl3^{-/-}$ mice was completely deleted in all tissues including WAT and iBAT (Figure 2A), with no influence on its paralogs *Ormdl1* and *Ormdl2* (data not shown). To test the effect of ORMDL3 on thermogenesis, $Ormdl3^{-/-}$ mice and their WT littermates were housed in a thermoneutral (30 °C) or cold (4 °C) environment for 2 weeks. $Ormdl3^{-/-}$ mice showed no phenotypic difference in body weight and adipose tissue weight compared to the WT mice in a thermoneutral environment (Supplemental Fig. S1). However, after 2 weeks of cold challenge, the weights of inguinal WAT (ingWAT) and epididymal WAT (eWAT) from $Ormdl3^{-/-}$ mice were significantly lower than those from WT littermate mice, whereas the body weight and iBAT weight of $Ormdl3^{-/-}$ mice were only slightly reduced (Supplemental Fig. S1). The decreased weight of ingWAT and eWAT in $Ormdl3^{-/-}$ mice caused by cold challenge needs to be further investigated. To test the physiological outcome of cold challenge, the mice were subjected to core body temperature analysis using a rectal probe. Although the body temperature of $Ormdl3^{-/-}$ mice at room temperature is comparable to that of WT mice, $Ormdl3^{-/-}$ mice failed to maintain their normal body temperature after 2 weeks of cold exposure. The average core body temperature of $Ormdl3^{-/-}$ mice was significantly decreased (from 37.5 ± 0.4 °C to 36.7 ± 0.5 °C) (Figure 2B). Next, the mice, which had been trained in a thermoneutral or cold environment, were kept at room temperature for 24 h to recover their body temperature

and then subjected to acute cold exposure. The mice that had been trained in a cold environment showed a higher core body temperature than the mice housed in a thermoneutral environment (Figure 2C), indicating that cold exposure had successfully activated the thermogenic response in mice. When subjected to acute cold exposure, the cold environment-trained *Ormdl3*$^{-/-}$ mice showed a rapid decrease in rectal temperature than the cold environment-trained WT mice (Figure 2C). These results indicated that cold-induced thermogenesis was impaired in mice lacking *Ormdl3*. We therefore examined the expression of genes associated with thermogenesis in iBAT harvested from *Ormdl3*$^{-/-}$ mice and their WT littermates. Cold exposure significantly induced the expression of thermogenic genes, including *Ucp1*, *PGC-1a*, *Elovl3, Prdm16*, and *Dio2,* whereas their expression was lower in *Ormdl3*$^{-/-}$ mice than in their WT littermates (Figure 2D). Western blotting and immunohistochemical staining showed that cold stress significantly increased UCP1 expression in the iBAT of WT mice, but the increased expression was significantly blunted in the iBAT of *Ormdl3*$^{-/-}$ mice (Figure 2E, F). Consistently, histological assessment revealed that cold exposure resulted in smaller adipocytes in the iBAT of WT mice, but the morphological change was attenuated in *Ormdl3*$^{-/-}$ mice (Figure 2F), indicating that cold-induced lipolysis and thermogenesis are impaired by *Ormdl3* deficiency. Taken together, these data demonstrate that the thermogenic function of BAT is impaired by the ablation of *Ormdl3*.

3.3. *Ormdl3* ablation reduces WAT browning

Cold exposure could also induce the formation of beige adipocytes. We therefore examined the browning/beiging of WAT in *Ormdl3*$^{-/-}$ and WT mice. As shown in Figure 3A, there were no obvious differences in the morphology of WAT, which was mainly composed of large adipocytes with unilocular lipid droplets, between *Ormdl3*$^{-/-}$ and WT mice in thermoneutral environment (Figure 3A). Under cold exposure, multiple multilocular adipocytes, which are typically associated with the browning process, were observed in WAT from WT mice. However, much fewer multilocular beige adipocytes were detected in WAT from *Ormdl3*$^{-/-}$ mice, indicating a defect in WAT browning (Figure 3A). The thermogenic activity of beige cells relies largely on the mitochondrial protein UCP1. As expected, immunohistochemical staining and Western blotting showed that cold stress significantly increased UCP1 expression in WAT of WT mice, but not in that of *Ormdl3*$^{-/-}$ mice (Figure 3B, C). Consistently, while cold challenge significantly induced the expression of thermogenic genes in WT mice, including *Ucp1, Prdm16, Cpt1a, Cox7a, Cox8b* and *Cidea,* this induction was markedly attenuated in *Ormdl3*$^{-/-}$ mice (Figure 3D). However, the expression of genes related to adipocyte differentiation showed no obvious difference between the WAT of WT and that of *Ormdl3*$^{-/-}$ mice (Supplemental Fig. S2). Taken together, these findings indicate that *Ormdl3* deficiency in mice led to cold intolerance likely, at least in part, due to a defect in activating the browning process in WAT following cold exposure.

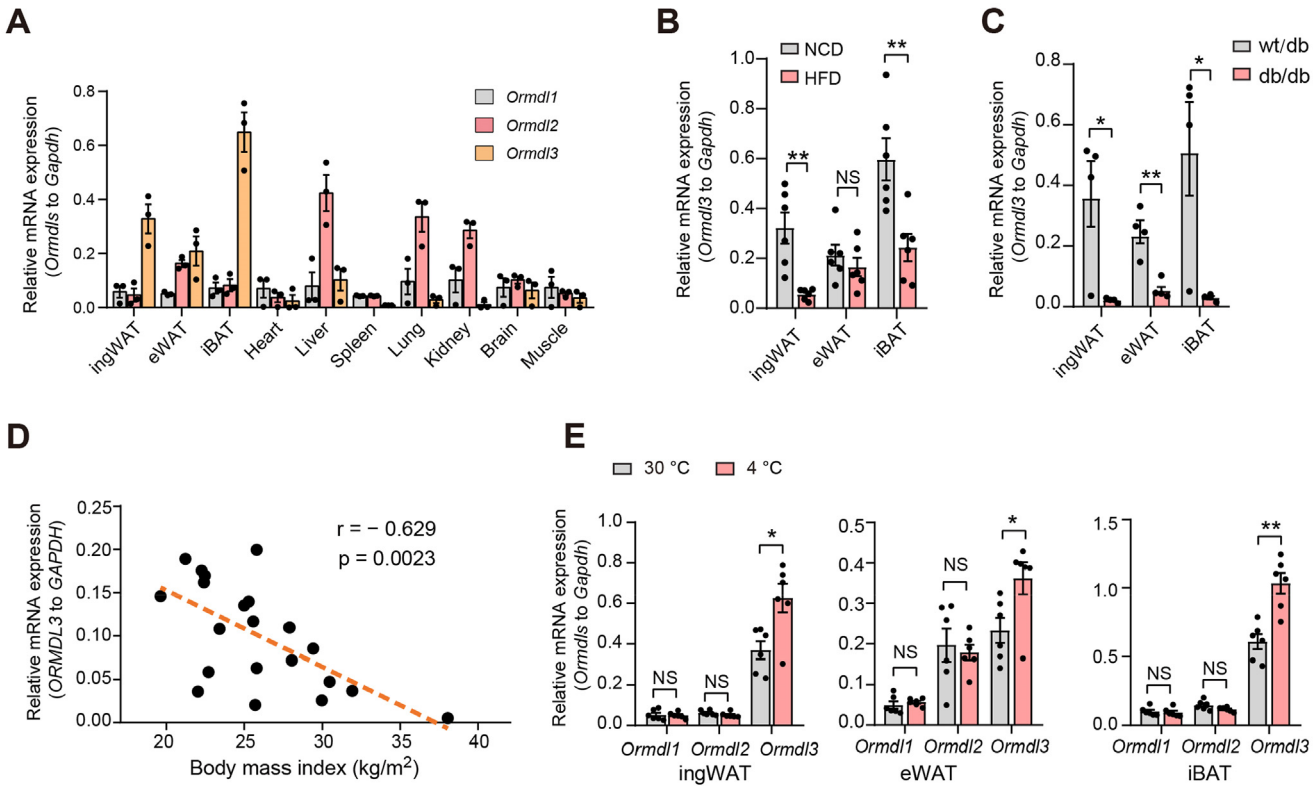

Figure 1: ORMDL3 is downregulated in obese mice and humans and upregulated in response to cold exposure. (A) The relative mRNA levels of *Ormdls* were determined in various tissues from 8-week-old male C57BL/6 mice. n = 3 mice per group. **(B)** The transcription of *Ormdl3* was downregulated in the adipose tissue of HFD-induced obese mice. Eight-week-old male C57BL/6 mice were fed a NCD or HFD for an additional 8 weeks, and the adipose tissue was then harvested and the relative *Ormdl3* expression was determined. n = 6 mice per group. **(C)** The relative mRNA levels of *Ormdl3* were determined in adipose tissues of *db/db* mice and their heterozygous littermates. n = 4 mice per group. (**D**) Negative correlation of *ORMDL3* mRNA levels in human subcutaneous adipose tissue with body mass index (n = 21). Correlation was assessed by the nonparametric Spearman test. **(E)** The transcription of *Ormdl3* was upregulated in the WAT and iBAT in response to cold exposure. n = 6 mice per group. The data in (**A**, **B**, **C** and **E**) are presented as mean ± SEM. NS, no significance; $*p < 0.05$, $**p < 0.01$ by unpaired nonparametric test.

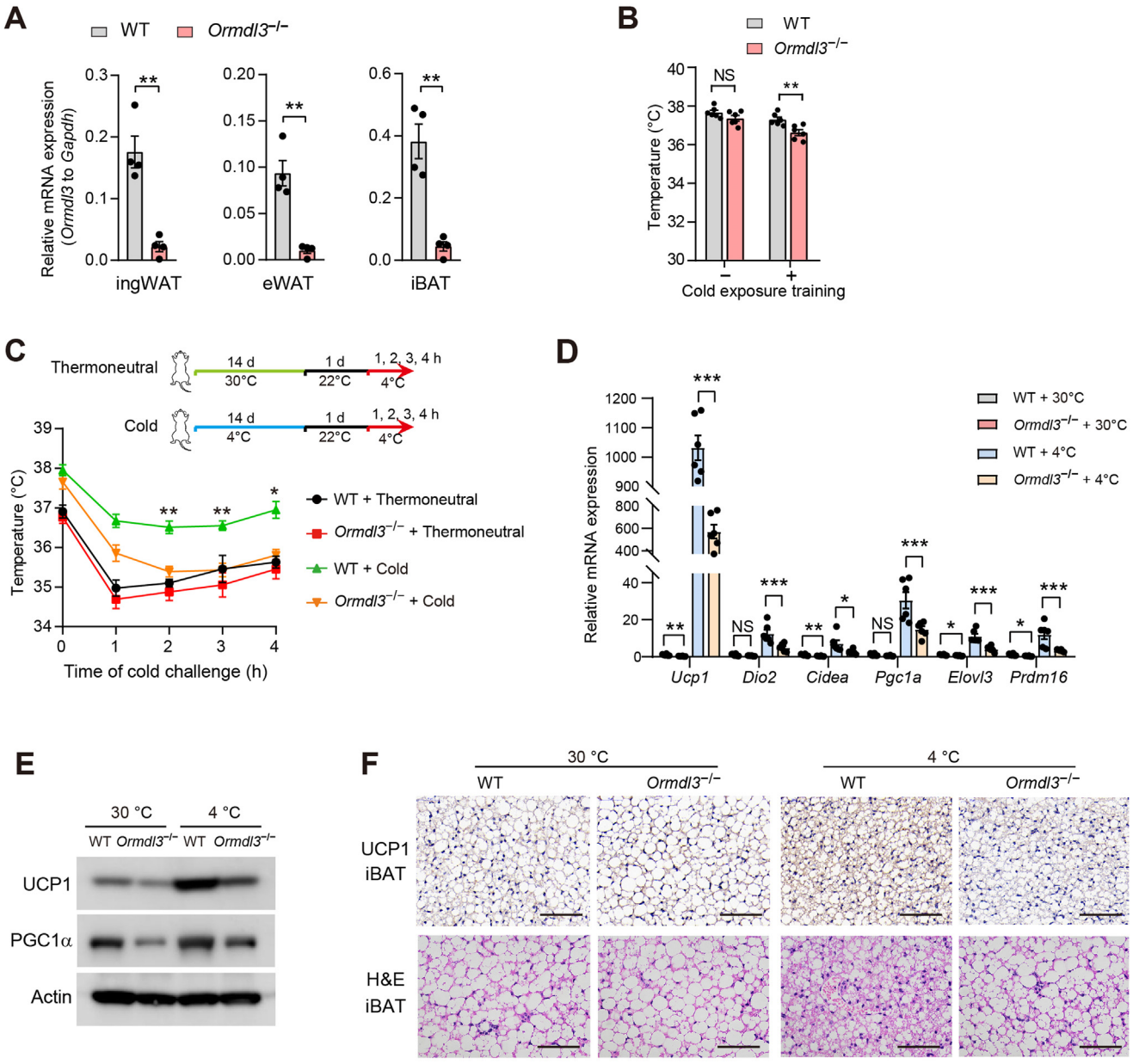

Figure 2: The thermogenic capacity of BAT is impaired in *Ormdl3* deficient mice. (A) The relative mRNA levels of *Ormdl3* in WAT and iBAT in *Ormdl3*$^{-/-}$ and WT mice (n = 4). **(B–F)** Eight-week-old *Ormdl3*$^{-/-}$ and their littermate WT mice (n = 6 mice per group) were housed at thermoneutral (30 °C) or exposed to cold environment (4 °C) for additional 2 weeks, and the following analysis was then performed: Body temperature in mice before and after cold challenge (**B**). The mice, which had been trained in thermoneutral or cold environment, were kept at room temperature for 24 h and then subjected to core body temperature analyses in acute cold exposure condition **(C)**. Quantitative PCR analysis of thermogenic gene expression in iBAT **(D)**. Western blot analysis of UCP1 and PGC1α protein levels in iBAT **(E)**. Representative H&E and immunohistochemical staining of iBAT (**F**). Scale bar, 100 μm. The data are presented as mean ± SEM. *P* values were determined by unpaired nonparametric test (**A**), one-way ANOVA (**B** and **D**) or two-way ANOVA with Šidák's multiple comparisons test (**C**, WT + 4 °C versus *Ormdl3*$^{-/-}$ + 4 °C). NS, no significance; $*p < 0.05$, $**p < 0.01$.

The stromal-vascular fraction from WAT contains fat progenitor cells that have the potential to differentiate into beige cells [21]. To examine whether ORMDL3 directly regulates adipocyte browning, we isolated the stromal-vascular fraction from ingWAT of *Ormdl3*$^{-/-}$ and WT mice and induced them to differentiate toward beige adipocytes. We found that while the morphological differentiation of precursor cells (Figure 3E) and the expression of general adipocyte markers (Figure 3F) were comparable, the induction of *Ucp1* and other thermogenic genes were less pronounced in the *Ormdl3*-deficient cells than in WT cells (Figure 3G). Collectively, these results indicate that ORMDL3 can promote beige adipocyte differentiation cell autonomously.

3.4. *Ormdl3* ablation reduces the response to adrenergic agonists

Cold exposure promotes brown/beige activation primarily through activation of the adrenergic signaling pathway [22]. To further confirm the effect of *Ormdl3* deficiency on brown/beige activation, we treated WT and *Ormdl3*$^{-/-}$ mice with the β3 adrenergic agonist CL-316243. CL-316243 treatment resulted in reduced adipocyte size and elevated expression of thermogenic genes in the BAT of WT mice. However, the

change in the morphology and the expression of thermogenic genes were significantly blunted in iBAT of *Ormdl3*$^{-/-}$ mice (Figure 4A—C). CL-316243 treatment induced many dense regions and multilocular adipocytes in the WAT of WT mice, which were typical phenotypes during WAT browning. In contrast, such morphologic changes were rarely observed in *Ormdl3*$^{-/-}$ mice (Figure 4D). Moreover, while UCP1 expression was dramatically increased by CL-316243 treatment in WT mice, it was only minimally induced in *Ormdl3*$^{-/-}$ mice (Figure 4E,F). In addition, we compared the expression levels of the key genes involved in adipose thermogenesis before and after CL-316243 injection. The induction of thermogenic genes by CL-316243 was severely blunted in *Ormdl3*$^{-/-}$ mice (Figure 4G). Taken together, these results suggest that *Ormdl3* deficiency also attenuated brown/beige cell activation caused by adrenergic signaling.

3.5. *Ormdl3*$^{-/-}$ mice are prone to HFD-induced obesity and systemic insulin resistance

The thermogenic program of brown/beige fat cells provides protection against metabolic disease and obesity [23]. We therefore tested the roles of *Ormdl3* in diet-induced obesity and insulin resistance. Eight-week-old *Ormdl3*$^{-/-}$ mice and their WT littermates were fed with HFD for additional 16 weeks. Under the HFD conditions, the body weight of *Ormdl3*$^{-/-}$ mice increased more pronouncedly than that of their WT littermates (Figure 5A). The iBAT and WAT masses were also significantly greater in *Ormdl3*$^{-/-}$ mice than in WT mice (Figure 5B—D). The increased adiposity in the HFD-fed animals was associated with a concomitant elevation in circulating leptin levels and the total serum cholesterol and triglyceride levels (Figure 5E).

Given that brown and beige fat contribute significantly to the regulation of glucose homeostasis. We next assessed the effects of *Ormdl3* deletion on glucose homeostasis and insulin sensitivity. HFD-induced glucose intolerance and insulin resistance in *Ormdl3*$^{-/-}$ mice were significantly enhanced compared to those in WT mice (Figure 5F,G). Consistent with the results of insulin tolerance test, HFD-fed *Ormdl3*$^{-/-}$ mice had higher levels of fasting insulin and free fatty acid, whereas the concentration of serum adiponectin was significantly lower than that in WT littermates (Figure 5H). Collectively, these results suggest that *Ormdl3* deficiency exacerbates the overall metabolic phenotypes associated with HFD-induced obesity.

We next sought to characterize the potential mechanisms underlying *Ormdl3* deficiency-induced obesity. *Ormdl3*$^{-/-}$ mice and WT mice had similar food intake (Figure 5I). Consistent with the data under NCD fed conditions, the thermogenic genes and UCP1 expression were significantly decreased in the iBAT of *Ormdl3*$^{-/-}$ mice fed a HFD (Figure 5J,K). In addition, histological analyses revealed fewer mitochondria in the adipose tissue of *Ormdl3*$^{-/-}$ mice (Supplemental Fig. S3). Taken together, these data indicate that *Ormdl3* deficiency exacerbates the obesity phenotypes by impairing the thermogenic capacity of brown fat.

3.6. *Ormdl3* ablation impairs brown/beige cell activation by increasing ceramide generation

Since lipids are the major constituents of adipocytes, their lipid composition plays a vital role in regulating adipocyte differentiation and function [24]. To test whether the deletion of *Ormdl3* impaired adipocyte browning by altering lipid composition of adipocytes, we conducted non-targeted lipidomics analysis of WAT from WT and *Ormdl3*$^{-/-}$ mice. As expected, the deletion of *Ormdl3* resulted in altered lipidomics profiles. Interestingly, ceramide species were significantly elevated in WAT from *Ormdl3*$^{-/-}$ mice compared to that from WT tissues (Figure 6A—D). These results are consistent with previous reports that ORMDL3 negatively regulates systemic ceramide levels [25—27].

Ceramide is a major hub of sphingolipid metabolism and has been reported to inhibit adipose browning [28,29]. To assess whether impaired WAT browning in *Ormdl3*$^{-/-}$ mice was mediated by increased ceramides, we employed myriocin to inhibit serine palmitoyltransferase (SPT), the rate-limiting enzyme of de novo ceramide synthesis [26,30], in the *in vitro* beige differentiation process. The reduction in the expression of thermogenic genes in *Ormdl3*$^{-/-}$ cells was attenuated by myriocin treatment (Figure 6E). To investigate the effects of ceramide production inhibition on thermal regulation, we administered myriocin to WT and *Ormdl3*$^{-/-}$ mice and then subjected them to core body temperature analyses under acute cold exposure conditions. The *Ormdl3*$^{-/-}$ mice showed a rapid decrease in rectal temperature compared to WT mice, whereas myriocin treatment significantly attenuated the decreased body temperature in *Ormdl3*$^{-/-}$ mice (Figure 6F).

Next, we determined the effect of pharmacological inhibition of ceramide production on CL-316243 induced brown/beige activation and thermal regulation. Myriocin treatment significantly rescued the decreased body temperature, whitening of iBAT and larger fat cell size of WAT in CL-316243-treated *Ormdl3*$^{-/-}$ mice (Figure 7A,B). Consistently, the UCP1 expression in CL-316243-treated *Ormdl3*$^{-/-}$ mice was upregulated in myriocin-treated groups (Figure 7C). These results suggested that the decrease in ceramide synthesis could improve the thermogenic capacity of *Ormdl3*$^{-/-}$ mice by promoting brown/beige cell activation.

We then monitored the effect of myriocin on the progression of diet-induced obesity in *Ormdl3*$^{-/-}$ and WT mice. Myriocin was administered to mildly obese (fed a HFD for 8 weeks) mice for an additional 8 weeks. As expected, the increase in HFD-induced body weight in *Ormdl3*$^{-/-}$ mice was attenuated by myriocin treatment. During the myriocin treatment period, the body weight of the vehicle group increased by 6.0 g, while the myriocin-treated groups gained only 2.2 g (Figure 7D). In addition, myriocin improved glucose disposal following exogenous insulin and glucose injection (Figure 7E). Furthermore, myriocin treatment also significantly upregulated the protein levels of UCP1 and PGC1α (Figure 7F), indicating that inhibition of ceramide synthesis in *Ormdl3*$^{-/-}$ mice can improve the overall metabolic condition. Taken together, these results suggest that *Ormdl3* ablation exacerbates obesity phenotypes through enhanced ceramide synthesis and impaired adipose tissue thermogenesis.

4. DISCUSSION

Igniting thermogenesis within adipose tissues has attracted major research interest over the last decade, as it may help to tackle obesity and improve metabolic health. *ORMDL3* is identified as an obesity-related gene, and its expression is negatively correlated with body mass index by genome-wide association studies [14]. In this study, we demonstrate that *Ormdl3* deficiency impairs BAT activation and white adipocyte browning, which decreases thermogenic capacity and exacerbates HFD-induced metabolic phenotypes by increasing ceramide generation. We have provided several lines of evidence to support this claim. First, the deletion of *Ormdl3* impaired the differentiation of preadipocytes into thermogenic beige adipocytes *in vitro*. Second, the lack of *Ormdl3* decreased BAT/beige cell activation under cold exposure or adrenergic agonist stimulation *in vivo*. Third, *Ormdl3*$^{-/-}$ mice exhibited increased susceptibility to HFD-induced obesity and insulin resistance. Fourth, increased levels of ceramides were detected in adipose tissue by lipidomics profiling. Finally, the inhibition of SPT, the

rate-limiting enzyme of de novo ceramide synthesis, by myriocin attenuated the reduction in thermogenic gene expression and the increase in HFD-induced body weight gain caused by *Ormdl3* deletion. Our results suggest that inhibiting ceramide production may ameliorate the metabolic disorders associated with *Ormdl3* deficiency.

A growing body of evidence has suggested the genetic association of *ORMDL3* polymorphisms with a diverse set of inflammatory disorders including bronchial asthma and inflammatory bowel disease [6,8]. Obesity is associated with chronic inflammation and is a common comorbidity in patients with asthma [31]. Incidence of inflammatory bowel

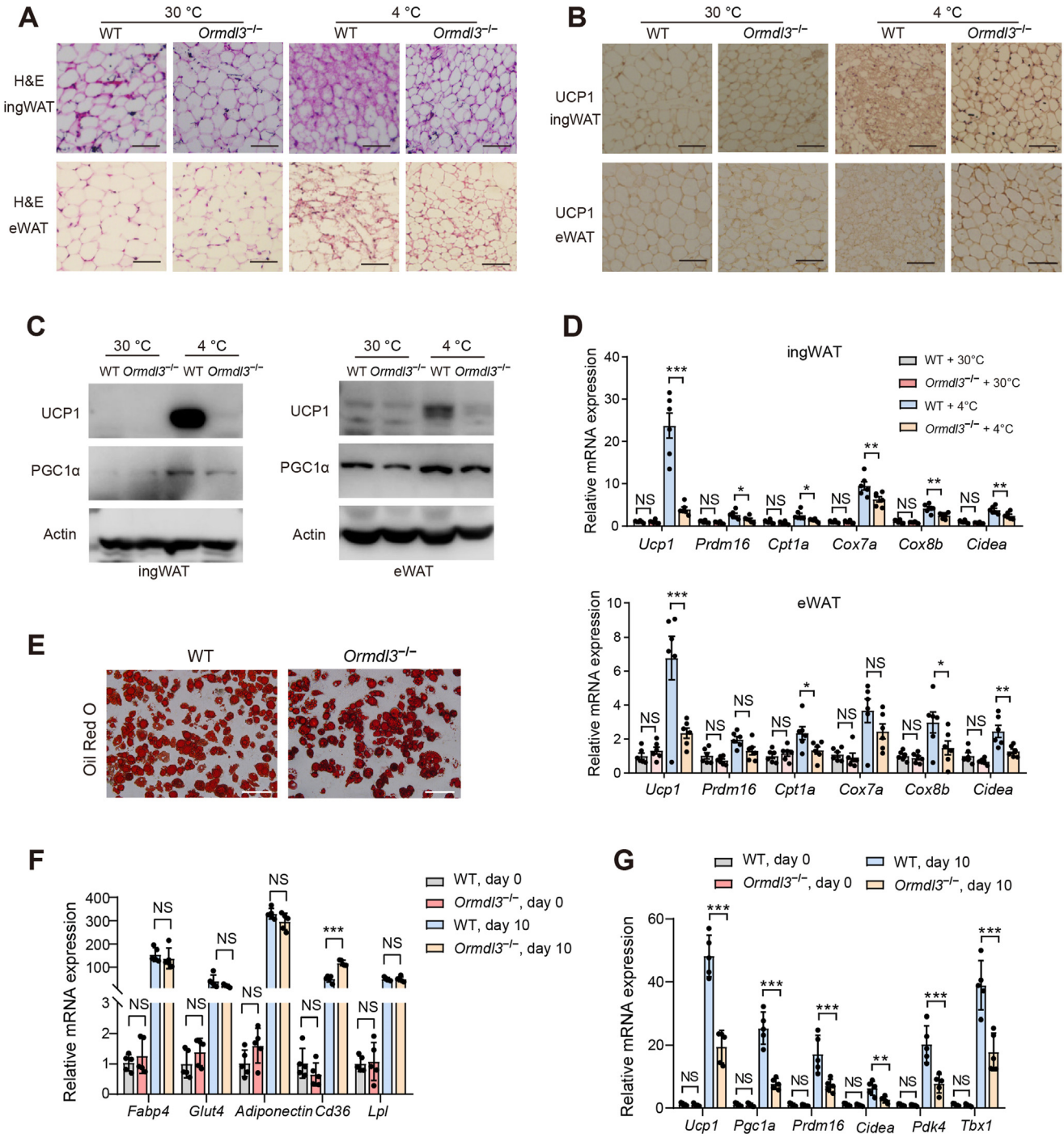

Figure 3: *Ormdl3* ablation decreases WAT browning. (A–D) Eight-week-old *Ormdl3*$^{-/-}$ and their littermate WT mice (n = 6 per group) were housed at thermoneutrality (30 °C) or exposed to cold environment (4 °C) for 2 weeks, and the following analysis was then performed: Representative H&E (**A**) and immunohistochemical **(B)** staining of ingWAT and eWAT. Western blot analysis of UCP1 and PGC1α protein levels **(C)**. Quantitative PCR analysis of thermogenic gene expression in ingWAT and eWAT **(D)**. **(E–G)** SVFs were isolated from ingWAT of 8-week-old *Ormdl3*$^{-/-}$ and WT mice which were housed at room temperature (n = 5 per group) and treated to induce beige adipocyte differentiation. Oil Red O staining of differentiated cells **(E)**. Quantitative PCR analysis of general adipocyte markers **(F)** and thermogenic genes **(G)**. The data are presented as mean ± SEM (**D**) or mean ± SD (**F** and **G**). NS means no significance, $*p < 0.05$, $**p < 0.01$, $***p < 0.001$ by one-way ANOVA. Scale bar, 100 μm.

disease also increases with overweight and obesity [32]. Previous studies have suggested that mammalian ORMDL3 contributes to the regulation of inflammation through multiple pathways, including endoplasmic reticulum stress, autophagy, apoptosis, and B lymphocyte fate determination [11,15,33]. Our results showed that genetic loss of *Ormdl3* in mice could exacerbate the overall obesity phenotypes by blocking the development of beige fat and thermogenesis of brown/beige fat. It is worthwhile to determine whether thermogenic brown/beige adipogenesis is involved in the development of inflammatory disorders such as bronchial asthma and inflammatory bowel disease.

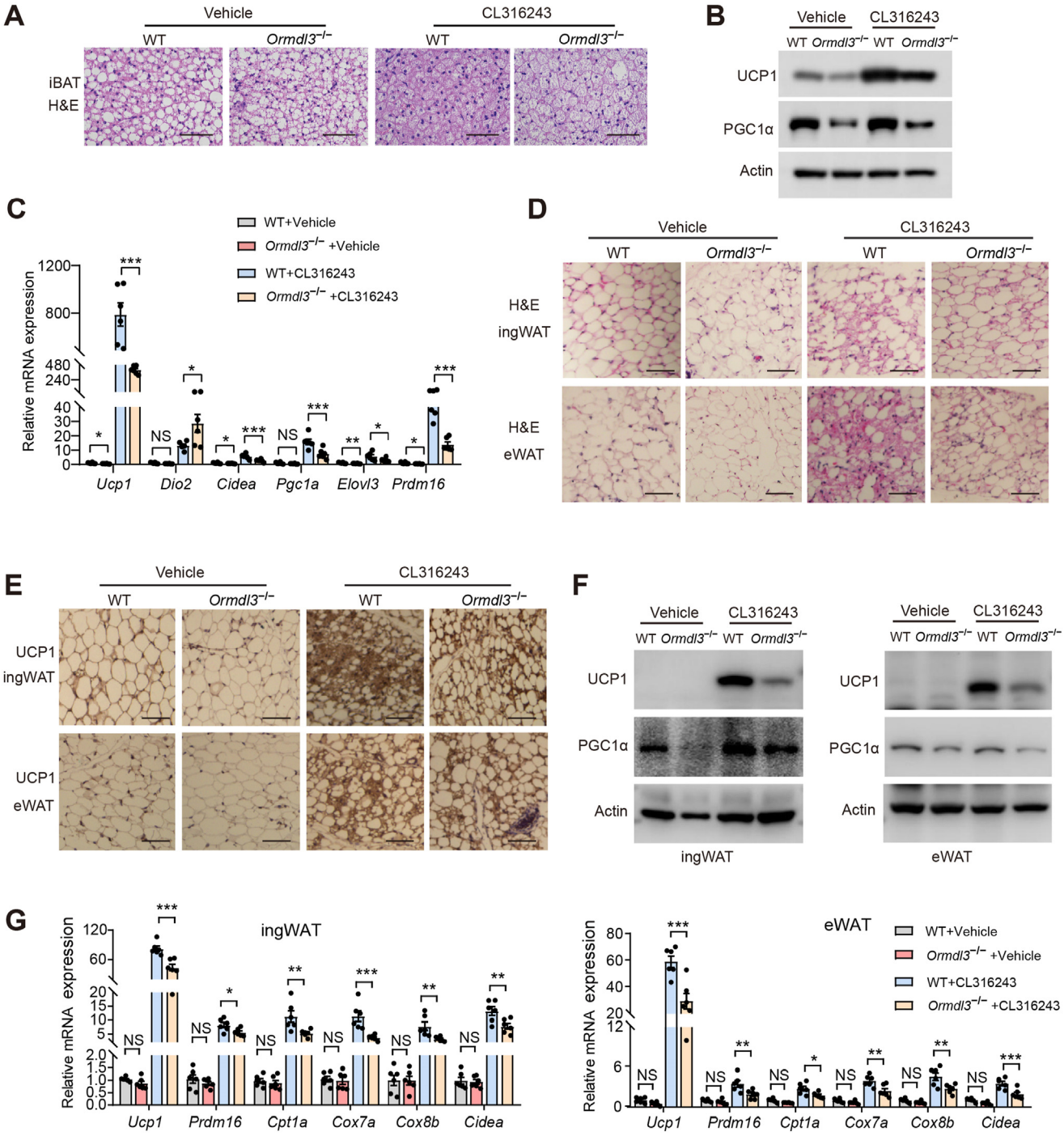

Figure 4: *Ormdl3* ablation reduces the response to adrenergic agonist. Eight-week-old *Ormdl3*$^{-/-}$ and their littermate WT mice were administered with β3 adrenergic agonist CL316243 or vehicle (n = 6 for each group), and the following analysis was then performed: **(A)** Representative H&E staining of iBAT. **(B)** Western blot analysis of UCP1 and PGC1α protein levels in iBAT. **(C)** Quantitative PCR analysis of thermogenic gene expression in iBAT. **(D–E)** Representative H&E (**D**) and immunohistochemical **(E)** staining of ingWAT and eWAT. **(F)** Western blot analysis of UCP1 and PGC1α protein levels in WAT. **(G)** Quantitative PCR analysis of brown/beige fat thermogenic gene expression in ingWAT and eWAT. The data are presented as mean ± SEM. NS means no significance, $*p < 0.05$, $**p < 0.01$, $***p < 0.001$ by one-way ANOVA. Scale bar, 100 μm.

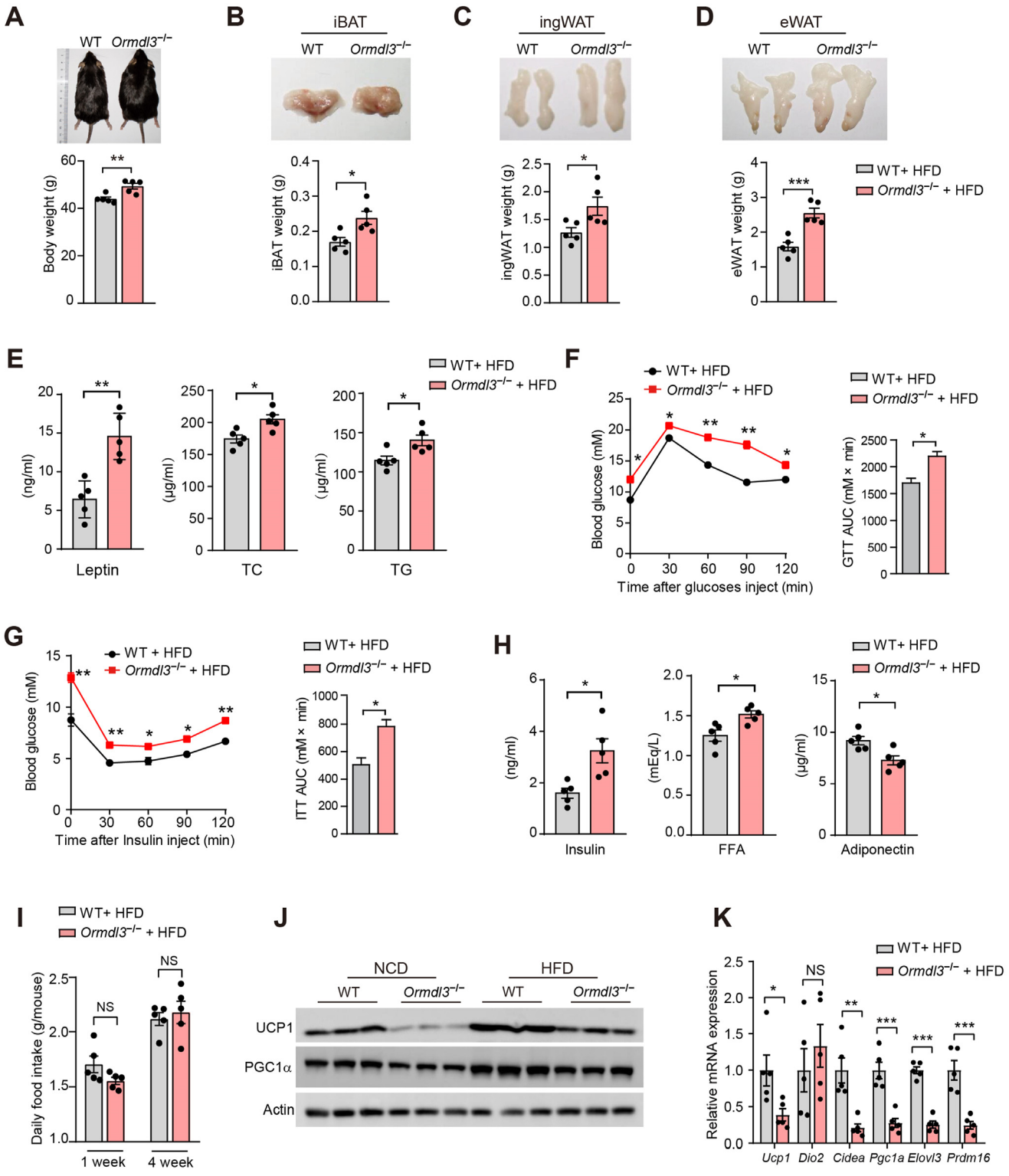

Figure 5: ***Ormdl3*** **ablation exacerbates HFD-induced obesity and insulin resistance.** Eight-week-old male WT and *Ormdl3*$^{-/-}$ mice were fed HFD for an additional 16 weeks at room temperature (22 °C). **(A–D)** Representative photographs of mice as well as fat pads (top). Body and fat pad weights in absolute amounts (bottom) (n = 5 mice per group). **(E)** Fasting plasma concentrations of leptin, total cholesterol, and triglyceride. **(F)** Glucose tolerance tests. **(G)** Insulin tolerance tests. **(H)** Fasting plasma concentrations of insulin, free fatty acid (FFA), and adiponectin. **(I)** Daily food intake was monitored during the first and fourth week during HFD feeding. **(J)** Western blot analysis of UCP1 and PGC1α protein levels in iBAT from NCD- and HFD-fed mice. **(K)** Quantitative PCR analysis of thermogenic gene expression in iBAT (n = 5). The data are presented as mean ± SEM. *P* values were determined by unpaired nonparametric test except (left of **F** and **G**) with two-way ANOVA with Šidák's multiple comparisons test. NS means no significance, $*p < 0.05$, $**p < 0.01$, $***p < 0.001$.

Given the wide variety of vital cellular roles of sphingolipids, their levels are tightly regulated. The first and rate-limiting step in de novo ceramide biosynthesis catalyzed by SPT is a key point of regulation. It has been conclusively demonstrated that yeast proteins ORM1 and ORM2 function as inhibitors of de novo sphingolipid synthesis by controlling the activity of SPT. However, mammalian ORMDLs lack the N-terminal phosphorylation site that is crucial for SPT regulation in yeast. Mammalian SPT activity seems to be affected only when all ORMDL paralogues are overexpressed or downregulated simultaneously. Studies addressing the regulation of SPT by individual ORMDLs generated conflicting conclusions. Using *Ormdl3* knockout and a transgenic mouse model, Debeuf et al. found that *Ormdl3* negatively regulated systemic ceramide levels, athough key asthma features were not altered [25]. By evaluating mice in which either one or combinations of two of the three *Ormdl* genes were deleted, researchers found that mice lacking both *Ormdl1* and *Ormdl3* exhibit highly elevated sphingolipid levels in the nervous system [34]. In contrast, other studies did not observe a consistent change in total sphingolipid levels in response to abolished or increased ORMDL3 expression [35]. In the present study, we evaluated the lipid composition of white adipose and found that 5 ceramides were elevated in *Ormdl3*$^{-/-}$ mice, supporting that *Ormdl3* deficiency is sufficient to upregulate ceramide levels. However, a normalization method that is not based on internal standards was applied in this lipidomics analysis.

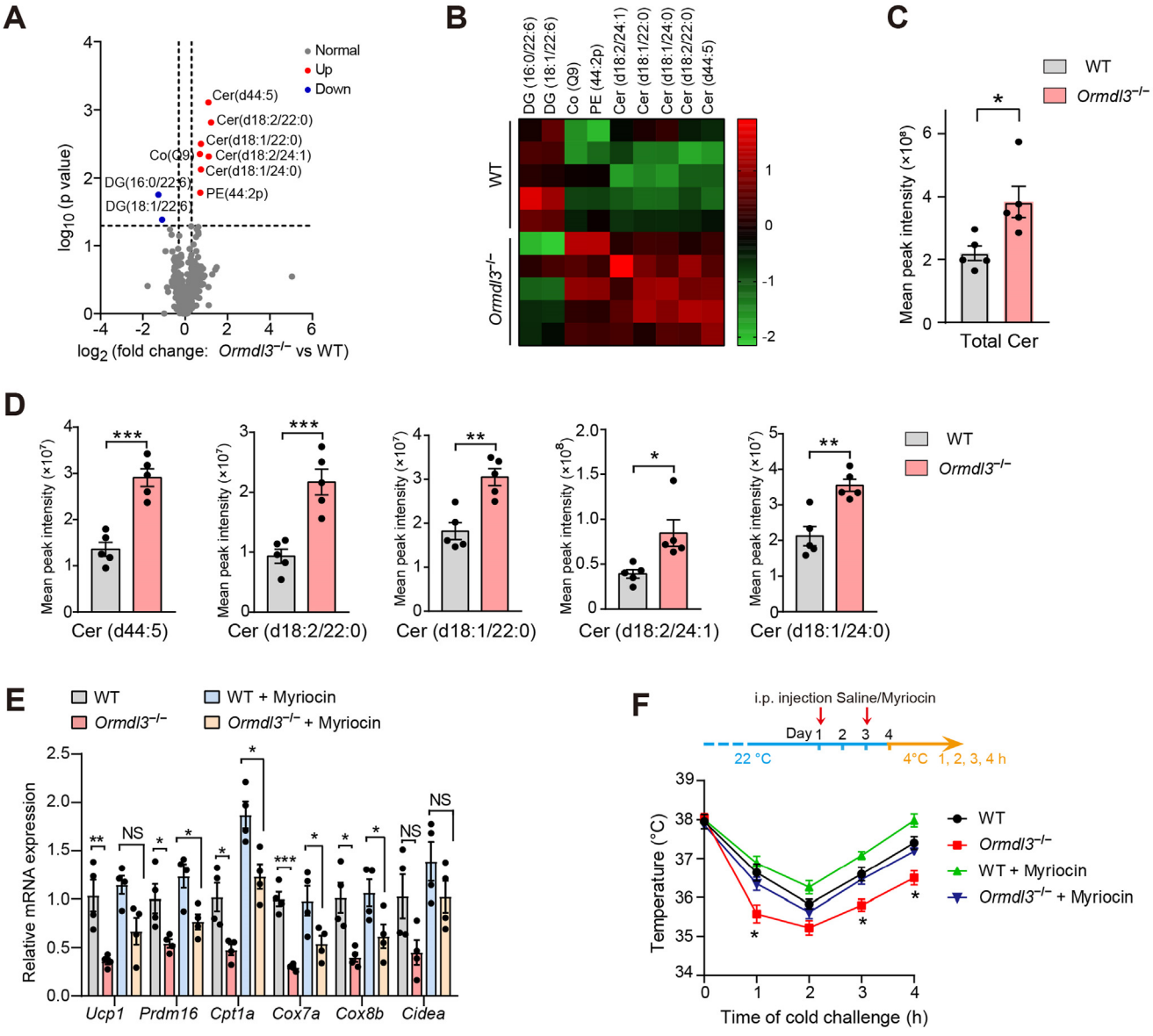

Figure 6: *Ormdl3* ablation impairs brown/beige cells activation through increasing ceramide generation. (A) Volcano plots showing fold-change and p-value for the comparison of lipids from *Ormdl3*$^{-/-}$ versus WT ingWAT based on the lipidomics data (n = 5). **(B)** Heatmap summarizing the lipids that were significantly different between WT and *Ormdl3*$^{-/-}$ mice. **(C–D)** Total ceramide (**C**) and several ceramides that were significantly different between WT and *Ormdl3*$^{-/-}$ mice (**D**) are shown. **(E)** Quantitative PCR analysis of brown/beige fat thermogenic gene expression in induced beige adipocyte (n = 4). **(F)** Eight-week-old male WT and *Ormdl3*$^{-/-}$ mice housed in room temperature were injected intraperitoneally with myriocin (0.3 mg/kg) or saline on day 1 and day 3. On the fourth day, the mice were subjected to core body temperature analyses in acute cold exposure condition (n = 6). The data are presented as mean ± SEM. *P* values were determined by unpaired nonparametric test (**C** and **D**), one-way ANOVA (**E**) or two-way ANOVA with Šidák's multiple comparisons test (**F**, WT versus *Ormdl3*$^{-/-}$). NS means no significance, $*p < 0.05$, $**p < 0.01$, $***p < 0.001$.

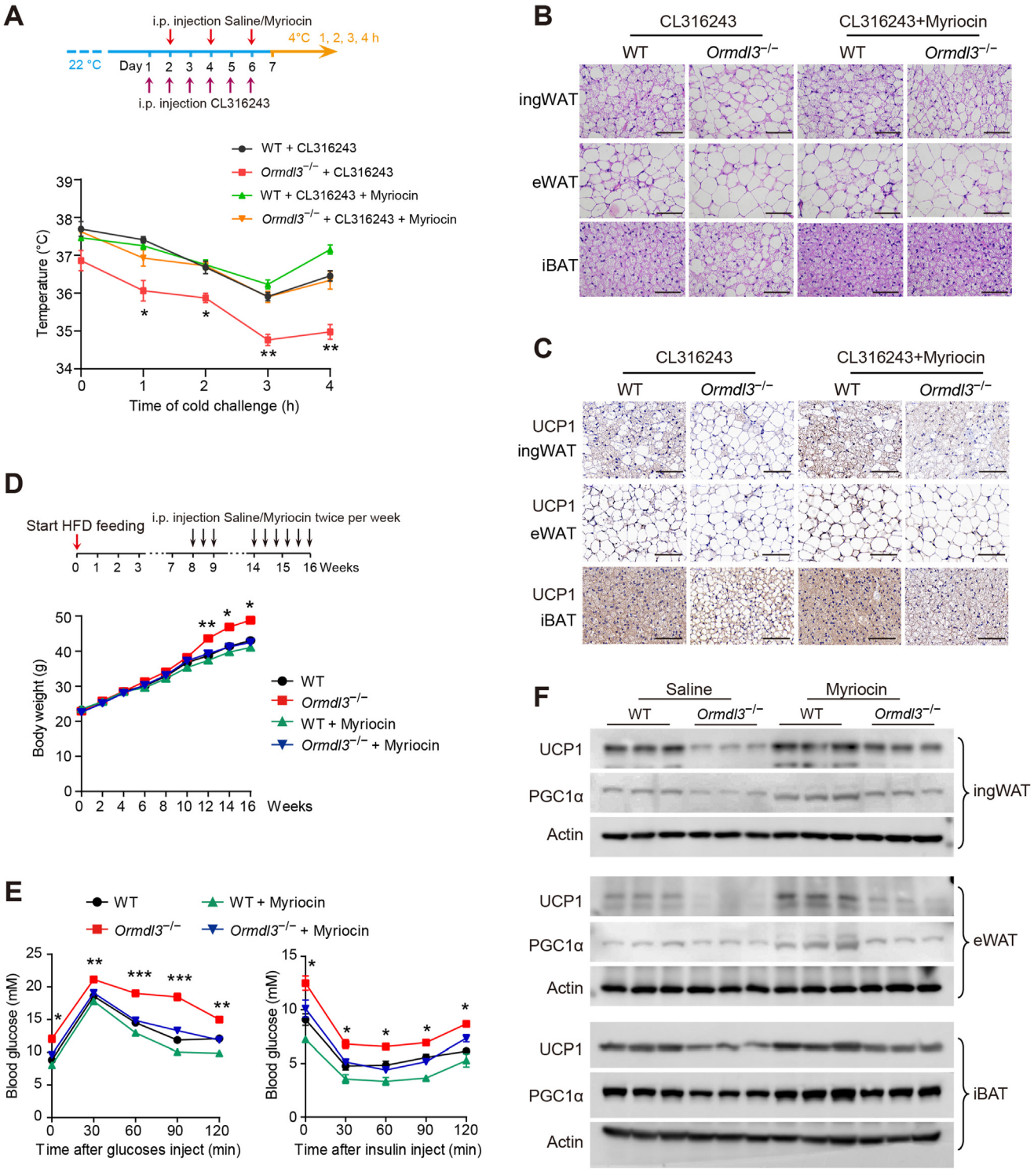

Figure 7: Blockage of ceramide generation reverses decreased thermogenesis and increased obesity phenotypes in Ormdl3−/− mice. (A–C) The *Ormdl3*$^{-/-}$ and their littermate WT mice were administered the β3 adrenergic agonist CL316243 plus myriocin or vehicle (n = 5 mice per group), and the body temperature change in mice was determined by cold challenge at 4 °C (**A**). Representative H&E (**B**) and immunohistochemical **(C)** staining of ingWAT, eWAT and iBAT. **(D–F)** Eight-week-old male WT and *Ormdl3*$^{-/-}$ mice were fed HFD for additional 16 weeks. From the 9th week, myriocin or saline was administered to mice twice per week. **(D)** Body weight of WT and *Ormdl3*$^{-/-}$ mice during 16 weeks (n = 6). **(E)** Left: Glucose tolerance tests. Right: Insulin tolerance tests (n = 5). **(F)** Western blot analysis of UCP1 and PGC1α protein levels. The data are presented as mean ± SEM. *P* values were determined by two-way ANOVA with Šidák's multiple comparisons test (**A,** WT + CL316243 versus *Ormdl3*$^{-/-}$ + CL316243; **D and E**, WT versus *Ormdl3*$^{-/-}$). NS means no significance, $^{*}p < 0.05$, $^{**}p < 0.01$, $^{***}p < 0.001$. Scale bar, 100 μm.

Hence, the observation of increased ceramides shown in Figure 6 was only semi-quantitative. We cannot exclude possible interferences from extraction loss and ion suppression. It is worthwhile to target these changed lipid molecules and quantify the absolute changes by using stable isotope-labeled internal standards in future studies.

Prior studies have shown that adipose ceramides are increased in people with obesity and correlate with insulin resistance and hepatic steatosis [36,37]. Inhibition of SPT activity by myriocin, a high-affinity inhibitor, blocks the synthesis of sphingolipids and prevents the development of insulin resistance and diabetes in obese mice and rats [28]. Consistently, induction of ceramide degradation also improves systemic metabolism and reduces hepatic steatosis. Recent studies indicate that sphingolipids are important nutrient modulators of the thermogenic and metabolic activity of adipocytes, particularly in subcutaneous WAT. While cold exposure increases the thermogenic capacity of adipocytes by elevating the expression of thermogenic genes such as *Ucp1*, *Pgc1a*, and *Prdm16*, and reduces ceramide, dihydroceramide, and sphinganine in adipose tissue as well as the expression of the ceramide biosynthetic genes *Sptlc2* and *CerS6* [28]. Systemic inhibition of ceramide biosynthesis or adipocyte-specific depletion of *Sptlc2* increases the recruitment of beige adipocytes in adipose tissue and improves mitochondrial function [29]. Consistent with these observations, we observed impaired browning capacity and elevated ceramide levels in the adipose tissue of *Ormdl3*$^{-/-}$ mice. Inhibition of ceramide production by myriocin could rescue the impaired browning and increased weight/fat gain caused by *Ormdl3* deletion. However, an adipocyte-specific *Ormdl3* deletion mouse model (generated by *adiponectin*-cre or *ucp1*-cre) in a thermoneutral or cold environment needs to be analyzed to further validate whether impaired adipose thermogenesis/browning accounts for HFD-induced obesity in *Ormdl3*$^{-/-}$ mice.

UCP1 dissipates energy in the form of heat by uncoupling cellular respiration and mitochondrial ATP synthesis. In our study, the UCP1 expression induced by cold exposure or β3 adrenergic agonist was severely blunted by *Ormdl3* ablation. Recently, Ikeda et al. reported a distinct non-canonical UCP1-independent thermogenic mechanism in beige adipocytes, which involved ATP-dependent Ca^{2+} cycling by sarco/endoplasmic reticulum Ca^{2+}-ATPase 2b (SERCA2b) and ryanodine receptor 2 [38]. Inhibition of SERCA2b impairs UCP1-independent beige fat thermogenesis in humans and mice. Conversely, enhanced Ca^{2+} cycling stimulates UCP1-independent thermogenesis in beige adipocytes [38]. However, Flicker et al. reported that the mice lacking uniporter-based calcium uptake in BAT mitochondria were unaffected in cold tolerance, diet-induced obesity, and transcriptional response to cold in BAT [39]. Previous studies reported that ORMDL3 regulates endoplasmic reticulum-mediated calcium signaling [11] and mitochondrial Ca^{2+} influx [40]. The regulatory role of ORMDL3 in Ca^{2+} cycling-mediated thermogenesis would be an intriguing topic for future studies.

In conclusion, we demonstrate that *Ormdl3* deficiency impairs BAT activation and white adipocyte browning by increasing ceramide generation. Mammalian ORMDLs do not contain the phosphorylation sites known to control their interaction with SPT. Future studies are needed to determine how ORMDL3 negatively regulates ceramide biosynthesis by decreasing the activity of SPT.

AUTHOR CONTRIBUTIONS

Y.S., W.Z., Y.G., and P.L. designed the study. Y.S., W.Z. L.Q., S.H., L.Y., M.W., and B.J. conducted experiments and performed data analysis. Y.S., W.Z., Y.G., and P.L. interpreted the data and wrote the manuscript. P.F., Q.L., and C.S. reviewed and edited the manuscript. Y.G. and P.L. supervised the project.

ACKNOWLEDGMENTS

This study was supported by grants from the National Natural Science Foundation of China (81571523 and 31872810) to Y.G., (81972682) to P.L., (31970559) to B.J., the Natural Science Foundation of Jiangsu Province (BK20211543) to P.L., the Natural Science Foundation of Shandong Province (ZR2016HZ01) to Y.G., and the Key Research Project of Shandong Province (2016GSF201143) to B.J.

CONFLICT OF INTEREST

The authors declare no competing financial interests.

APPENDIX A. SUPPLEMENTARY DATA

Supplementary data to this article can be found online at https://doi.org/10.1016/j.molmet.2021.101423.

REFERENCES

[1] G.B.D.O. Collaborators, Afshin, A., Forouzanfar, M.H., Reitsma, M.B., Sur, P., Estep, K., Lee, A., et al., 2017. Health effects of overweight and obesity in 195 countries over 25 years. New England Journal of Medicine 377(1):13–27.

[2] Wang, W., Seale, P., 2016. Control of brown and beige fat development. Nature Reviews Molecular Cell Biology 17(11):691–702.

[3] Fedorenko, A., Lishko, P.V., Kirichok, Y., 2012. Mechanism of fatty-acid-dependent UCP1 uncoupling in brown fat mitochondria. Cell 151(2):400–413.

[4] Pan, R., Zhu, X., Maretich, P., Chen, Y., 2020. Metabolic improvement via enhancing thermogenic fat-mediated non-shivering thermogenesis: from rodents to humans. Frontiers in Endocrinology 11:633.

[5] Sidossis, L., Kajimura, S., 2015. Brown and beige fat in humans: thermogenic adipocytes that control energy and glucose homeostasis. Journal of Clinical Investigation 125(2):478–486.

[6] Moffatt, M.F., Kabesch, M., Liang, L.M., Dixon, A.L., Strachan, D., Heath, S., et al., 2007. Genetic variants regulating ORMDL3 expression contribute to the risk of childhood asthma. Nature 448(7152):470. U5.

[7] Saleh, N.M., Raj, S.M., Smyth, D.J., Wallace, C., Howson, J.M.M., Bell, L., et al., 2011. Genetic association analyses of atopic illness and proinflammatory cytokine genes with type 1 diabetes. Diabetes-Metab Res 27(8):838–843.

[8] McGovern, D.P.B., Gardet, A., Torkvist, L., Goyette, P., Essers, J., Taylor, K.D., et al., 2010. Genome-wide association identifies multiple ulcerative colitis susceptibility loci. Nature Genetics 42(4):332. U88.

[9] Laukens, D., Georges, M., Libioulle, C., Sandor, C., Mni, M., Vander Cruyssen, B., et al., 2010. Evidence for significant overlap between common risk variants for crohn's disease and ankylosing spondylitis. PLoS One 5(11).

[10] Ma, X.C., Qiu, R.F., Dang, J., Li, J.X., Hu, Q., Shan, S., et al., 2015. ORMDL3 contributes to the risk of atherosclerosis in Chinese Han population and mediates oxidized low-density lipoprotein-induced autophagy in endothelial cells. Scientific Reports 5.

[11] Cantero-Recasens, G., Fandos, C., Rubio-Moscardo, F., Valverde, M.A., Vicente, R., 2010. The asthma-associated ORMDL3 gene product regulates endoplasmic reticulum-mediated calcium signaling and cellular stress. Human Molecular Genetics 19(1):111–121.

[12] Hsu, K.J., Turvey, S.E., 2013. Functional analysis of the impact of ORMDL3 expression on inflammation and activation of the unfolded protein response in human airway epithelial cells. Allergy, Asthma and Clinical Immunology 9(1):4.

[13] Miller, M., Tam, A.B., Cho, J.Y., Doherty, T.A., Pham, A., Khorram, N., et al., 2012. ORMDL3 is an inducible lung epithelial gene regulating metalloproteases, chemokines, OAS, and ATF6. Proceedings of the National Academy of Sciences of the United States of America 109(41):16648–16653.

[14] Pan, D.Z., Garske, K.M., Alvarez, M., Bhagat, Y.V., Boocock, J., Nikkola, E., et al., 2018. Integration of human adipocyte chromosomal interactions with adipose gene expression prioritizes obesity-related genes from GWAS. Nature Communications 9(1):1512.

[15] Dang, J., Bian, X., Ma, X., Li, J., Long, F., Shan, S., et al., 2017. ORMDL3 facilitates the survival of splenic B cells via an ATF6alpha-endoplasmic reticulum stress-beclin1 autophagy regulatory pathway. The Journal of Immunology 199(5):1647–1659.

[16] Wen, B., Mei, Z., Zeng, C., Liu, S., 2017. metaX: a flexible and comprehensive software for processing metabolomics data. BMC Bioinformatics 18(1):183.

[17] Hrydziuszko, O., Viant, M.R., 2012. Missing values in mass spectrometry based metabolomics: an undervalued step in the data processing pipeline. Metabolomics 8(1):S161–S174.

[18] Di Guida, R., Engel, J., Allwood, J.W., Weber, R.J., Jones, M.R., Sommer, U., et al., 2016. Non-targeted UHPLC-MS metabolomic data processing methods: a comparative investigation of normalisation, missing value imputation, transformation and scaling. Metabolomics 12:93.

[19] Westerhuis, J.A., Hoefsloot, H.C.J., Smit, S., Vis, D.J., Smilde, A.K., van Velzen, E.J.J., et al., 2008. Assessment of PLSDA cross validation. Metabolomics 4(1):81–89.

[20] Barker, M., Rayens, W., 2003. Partial least squares for discrimination. Journal of Chemometrics 17(3):166–173.

[21] Harms, M., Seale, P., 2013. Brown and beige fat: development, function and therapeutic potential. Nature Medicine 19(10):1252–1263.

[22] Himms-Hagen, J., Melnyk, A., Zingaretti, M.C., Ceresi, E., Barbatelli, G., Cinti, S., 2000. Multilocular fat cells in WAT of CL-316243-treated rats derive directly from white adipocytes. American Journal of Physiology - Cell Physiology 279(3):C670–C681.

[23] Kajimura, S., Spiegelman, B.M., Seale, P., 2015. Brown and beige fat: physiological roles beyond heat generation. Cell Metabolism 22(4):546–559.

[24] Leiria, L.O., Tseng, Y.H., 2020. Lipidomics of brown and white adipose tissue: implications for energy metabolism. Biochimica et Biophysica Acta (BBA) - Molecular and Cell Biology of Lipids 1865(10):158788.

[25] Debeuf, N., Zhakupova, A., Steiner, R., Van Gassen, S., Deswarte, K., Fayazpour, F., et al., 2019. The ORMDL3 asthma susceptibility gene regulates systemic ceramide levels without altering key asthma features in mice. The Journal of Allergy and Clinical Immunology 144(6):1648–1659 e9.

[26] Cai, L., Oyeniran, C., Biswas, D.D., Allegood, J., Milstien, S., Kordula, T., et al., 2016. ORMDL proteins regulate ceramide levels during sterile inflammation. The Journal of Lipid Research 57(8):1412–1422.

[27] Li, S., Xie, T., Liu, P., Wang, L., Gong, X., 2021. Structural insights into the assembly and substrate selectivity of human SPT-ORMDL3 complex. Nature Structural & Molecular Biology 28(3):249–257.

[28] Chaurasia, B., Kaddai, V.A., Lancaster, G.I., Henstridge, D.C., Sriram, S., Galam, D.L.A., et al., 2016. Adipocyte ceramides regulate subcutaneous adipose browning, inflammation, and metabolism. Cell Metabolism 24(6):820–834.

[29] Chaurasia, B., Ying, L., Talbot, C.L., Maschek, J.A., Cox, J., Schuchman, E.H., et al., 2021. Ceramides are necessary and sufficient for diet-induced impairment of thermogenic adipocytes. Molecular Metabolism 45:101145.

[30] Breslow, D.K., Collins, S.R., Bodenmiller, B., Aebersold, R., Simons, K., Shevchenko, A., et al., 2010. Orm family proteins mediate sphingolipid homeostasis. Nature 463(7284):1048–1053.

[31] Miethe, S., Karsonova, A., Karaulov, A., Renz, H., 2020. Obesity and asthma. The Journal of Allergy and Clinical Immunology 146(4):685–693.

[32] Singh, S., Dulai, P.S., Zarrinpar, A., Ramamoorthy, S., Sandborn, W.J., 2017. Obesity in IBD: epidemiology, pathogenesis, disease course and treatment outcomes. Nature Reviews Gastroenterology & Hepatology 14(2):110–121.

[33] Ma, X., Long, F., Yun, Y., Dang, J., Wei, S., Zhang, Q., et al., 2018. ORMDL3 and its implication in inflammatory disorders. Int J Rheum Dis 21(6):1154–1162.

[34] Clarke, B.A., Majumder, S., Zhu, H., Lee, Y.T., Kono, M., Li, C., et al., 2019. The Ormdl genes regulate the sphingolipid synthesis pathway to ensure proper myelination and neurologic function in mice. Elife 8.

[35] Zhakupova, A., Debeuf, N., Krols, M., Toussaint, W., Vanhoutte, L., Alecu, I., et al., 2016. ORMDL3 expression levels have no influence on the activity of serine palmitoyltransferase. The FASEB Journal : Official Publication of the Federation of American Societies for Experimental Biology 30(12):4289–4300.

[36] Chaurasia, B., Summers, S.A., 2015. Ceramides - lipotoxic inducers of metabolic disorders. Trends Endocrin Met 26(10):538–550.

[37] Haus, J.M., Kashyap, S.R., Kasumov, T., Zhang, R.L., Kelly, K.R., DeFronzo, R.A., et al., 2009. Plasma ceramides are elevated in obese subjects with type 2 diabetes and correlate with the severity of insulin resistance. Diabetes 58(2):337–343.

[38] Ikeda, K., Kang, Q., Yoneshiro, T., Camporez, J.P., Maki, H., Homma, M., et al., 2017. UCP1-independent signaling involving SERCA2b-mediated calcium cycling regulates beige fat thermogenesis and systemic glucose homeostasis. Nature Medicine 23(12):1454–1465.

[39] Flicker, D., Sancak, Y., Mick, E., Goldberger, O., Mootha, V.K., 2019. Exploring the in vivo role of the mitochondrial calcium uniporter in Brown fat bioenergetics. Cell Reports 27(5):1364–1375 e5.

[40] Carreras-Sureda, A., Cantero-Recasens, G., Rubio-Moscardo, F., Kiefer, K., Peinelt, C., Niemeyer, B.A., et al., 2013. ORMDL3 modulates store-operated calcium entry and lymphocyte activation. Human Molecular Genetics 22(3):519–530.

